

University of Groningen

## Correlating the Influence of Disulfides in Monolayers across Photoelectron Spectroscopy Wettability and Tunneling Charge- Transport

Kumar, Sumit; Soni, Saurabh; Danowski, Wojciech; van Beek, Carlijn L. F.; Feringa, Ben L.; Rudolf, Petra; Chiechi, Ryan C.

*Published in:*  
Journal of the American Chemical Society

*DOI:*  
[10.1021/jacs.0c06508](https://doi.org/10.1021/jacs.0c06508)

**IMPORTANT NOTE: You are advised to consult the publisher's version (publisher's PDF) if you wish to cite from it. Please check the document version below.**

*Document Version*  
Publisher's PDF, also known as Version of record

*Publication date:*  
2020

[Link to publication in University of Groningen/UMCG research database](#)

*Citation for published version (APA):*

Kumar, S., Soni, S., Danowski, W., van Beek, C. L. F., Feringa, B. L., Rudolf, P., & Chiechi, R. C. (2020). Correlating the Influence of Disulfides in Monolayers across Photoelectron Spectroscopy Wettability and Tunneling Charge- Transport. *Journal of the American Chemical Society*, 142(35), 15075-15083. <https://doi.org/10.1021/jacs.0c06508>

### Copyright

Other than for strictly personal use, it is not permitted to download or to forward/distribute the text or part of it without the consent of the author(s) and/or copyright holder(s), unless the work is under an open content license (like Creative Commons).

### Take-down policy

If you believe that this document breaches copyright please contact us providing details, and we will remove access to the work immediately and investigate your claim.

*Downloaded from the University of Groningen/UMCG research database (Pure): <http://www.rug.nl/research/portal>. For technical reasons the number of authors shown on this cover page is limited to 10 maximum.*

# Correlating the Influence of Disulfides in Monolayers across Photoelectron Spectroscopy Wettability and Tunneling Charge-Transport

Sumit Kumar, Saurabh Soni, Wojciech Danowski, Carlijn L. F. van Beek, Ben L. Feringa, Petra Rudolf,\* and Ryan C. Chiechi\*



Cite This: *J. Am. Chem. Soc.* 2020, 142, 15075–15083



Read Online

ACCESS |



Metrics & More

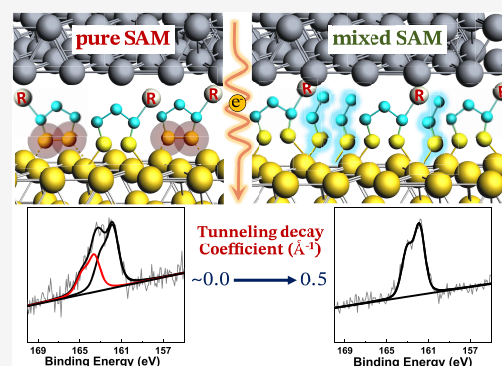


Article Recommendations



Supporting Information

**ABSTRACT:** Despite their ubiquity, self-assembled monolayers (SAMs) of thiols on coinage metals are difficult to study and are still not completely understood, particularly with respect to the nature of thiol–metal bonding. Recent advances in molecular electronics have highlighted this deficiency due to the sensitivity of tunneling charge-transport to the subtle differences in the overall composition of SAMs and the chemistry of their attachment to surfaces. These advances have also challenged assumptions about the spontaneous formation of covalent thiol–metal bonds. This paper describes a series of experiments that correlate changes in the physical properties of SAMs to photoelectron spectroscopy to unambiguously assign binding energies of noncovalent interactions to physisorbed disulfides. These disulfides can be converted to covalent metal–thiolate bonds by exposure to free thiols, leading to the remarkable observation of the total loss and recovery of length-dependent tunneling charge-transport. The identification and assignment of physisorbed disulfides solve a long-standing mystery and reveal new, dynamic properties in SAMs of thiols.



## INTRODUCTION

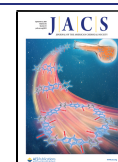
Organic monolayer films have found a wide variety of applications in the fields of chemistry, physics, molecular biology, biomedical engineering, and materials science,<sup>1–3</sup> including nanopatterning,<sup>4,5</sup> molecular-scale devices,<sup>6,7</sup> optical materials,<sup>8,9</sup> biosurfaces,<sup>10</sup> adhesion,<sup>11</sup> wettability,<sup>12</sup> and corrosion.<sup>13</sup> Self-assembled monolayers (SAMs) of thiols on gold are a particularly versatile and well-studied class of organic monolayer films that leverage the two-dimensional (2D) self-assembly of organic molecules mediated by the strong, but reversible, binding of thiols to metal surfaces.<sup>14–19</sup> The structural and interfacial properties of derivatives of alkanethiols in mixed monolayers were recently found to be closely related to the transport properties of tunneling junctions.<sup>20–26</sup> The special nature of this type of bonding is what imparts SAMs with some of their most useful properties, because it governs the dynamics of self-assembly and allows for the formation of densely packed monolayers as well as self-repair, in-place exchange, the formation of mixed monolayers, and responsiveness. Elucidating the special nature of covalent Au–S bonding on surfaces has, however, proven challenging.<sup>1</sup> Studies of the stability of thiol-based SAMs under various conditions of SAM formation, such as pH,<sup>27</sup> solvent effect,<sup>28</sup> influence of the roughness<sup>29</sup> of Au substrates, photo-irradiation,<sup>30</sup> effects of redox environments,<sup>31</sup> etc., provide insight into the self-assembly process. Optical tweezers,

magnetic tweezers, and single-molecule force spectroscopy<sup>32</sup> provide information about the properties of individual thiols bound to Au. It is, however, particularly challenging to investigate the nature of Au–S bonds in a SAM in a context in which it is useful, for example, on a macroscopic substrate under ambient conditions because they are, ultimately, self-assembled nanomaterials.<sup>2</sup>

The central challenge to studying large-area SAMs (as opposed to single-molecule or nanoscopic areas on Au single-crystals) is that they are heterogeneous and can comprise different types of Au–S bonds that affect the properties of the SAM. For example, thiolated-DNA physisorbed on Au as either Au···SH–R or Au···(S–S)···Au (where “–” represents a covalent bond, and “···” represents a noncovalent interaction; see Figure 1) resulted in SAMs with different properties than SAMs of the same thiolated-DNA comprising only covalent interactions.<sup>33</sup> Similarly, it has been shown that growing SAMs from solutions containing differing fractions of disulfides (S–S

Received: June 16, 2020

Published: August 10, 2020



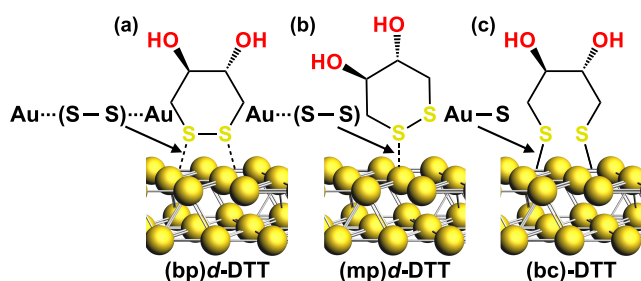


**Figure 1.** Three modes by which d-DTT can bind to Au: bidentate-physisorbed ((bp)d-DTT), monodentate-physisorbed ((mp)d-DTT), and bidentate-chemisorbed ((bc)-DTT) where “–” and “...” represent covalent and noncovalent interactions, respectively, and d stands for a dimerized S–S bond.

bonds) alters the rectification ratio in large-area tunneling junctions.<sup>34</sup> Likewise, there is also evidence that disulfide and thiol molecules pack and orient differently on Au.<sup>35</sup> In the field of molecular electronics, which is sensitive to small perturbations in structure/bonding, the nature and influence of Au–S bond(s) at the electrode interface are still not well understood. In their pioneering work on SAMs of thiols, Nuzzo et al. observed that S–S bonds are reduced spontaneously on Au surfaces to form Au–S bonds, finding no evidence of residual S–S bonds.<sup>14,15</sup> Subsequently, Whitesides et al. observed that thiols out-compete disulfides in the formation of SAMs and again did not observe any residual S–S bond.<sup>17</sup> However, Venkataraman et al. observed that, in single-molecule junctions, covalent Au–S and noncovalent Au... (S–S)... Au/Au...SH–R bonds affect injection currents differently, from which they further concluded

that Au... (S–S)... Au and Au...SH–R interactions can coexist in SAMs formed from thiols.<sup>36</sup> In this paper, we reconcile the apparent discrepancies in the nature of gold–thiolate binding that have been revealed by molecular–electronic studies and overcome a long-standing challenge to spectroscopic studies on SAMs by unambiguously identifying and assigning Au... (S–S)... Au bonds using photoelectron spectroscopy and correlating their presence to transport properties in tunneling junctions comprising SAMs.

X-ray photoelectron spectroscopy (XPS) is a powerful tool for identifying chemical species in SAMs. It can provide information about Au–S interactions, characterize the average thicknesses of monolayers, elucidate the tilt angles of molecules with respect to the surface normal, and determine the orientation and vertical positions of functional groups. In short, XPS is a comprehensive spectroscopy for interrogating SAMs of thiols.<sup>37</sup> In the S 2p core level of an XPS spectrum at binding energies of 161.8–162.0 eV, an S 2p<sub>3/2</sub> peak corresponds to a Au–S covalent bond. Shifts in this range of binding energies correspond to changes in the oxidation state of the sulfur atom, reflecting changes in interactions between Au and S, whether they be covalent or noncovalent in nature. However, in several XPS and high-resolution (HR) XPS studies (at a resolution limit of 0.05 eV),<sup>33,35</sup> Au... (S–S)... Au and Au...SH–R interactions have been interchangeably assigned to the same binding energies, ranging from 163 to 164 eV, e.g., a commonly occurring S 2p<sub>3/2</sub> peak at (163.6 ± 0.2) eV.<sup>38–42</sup> The ambiguity of this assignment limits XPS to a qualitative measure of the quality of a SAM; a high-quality SAM lacks a peak at (163.6 ± 0.2) eV because it can only be ascribed to noncovalent binding. The assignment

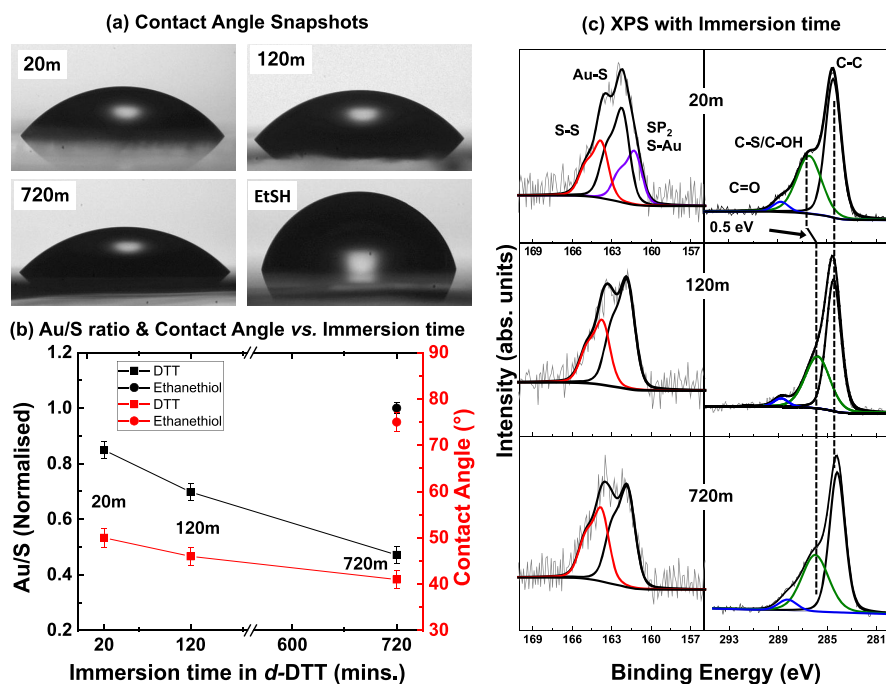


**Figure 2.** (a) Water contact angles on SAMs of pure DTT grown from d-DTT with immersion times of 20 min (20m), 120 min (120m), and 720 min (720m). Contact angles of SAM of pure ethanethiol (EtSH) serve as a reference. (b) Water contact angles (red) and normalized Au/S ratios from XPS (black) versus the immersion time for SAMs of DTT (squares) and EtSH (circles). (c) XPS spectra of the SAMs 20m, 120m, 720m. The left column shows the corresponding S 2p core-level spectra, which comprise multiple doublets corresponding to Au–S bonds (black curve), hollow-site bonds (purple curve), and S–S bonds (red curve). The right column shows the C 1s core-level spectra, which comprise peaks corresponding to C–C bonds (black curve), C–S/C–OH bonds (green curve), and C=O bonds (blue curve).

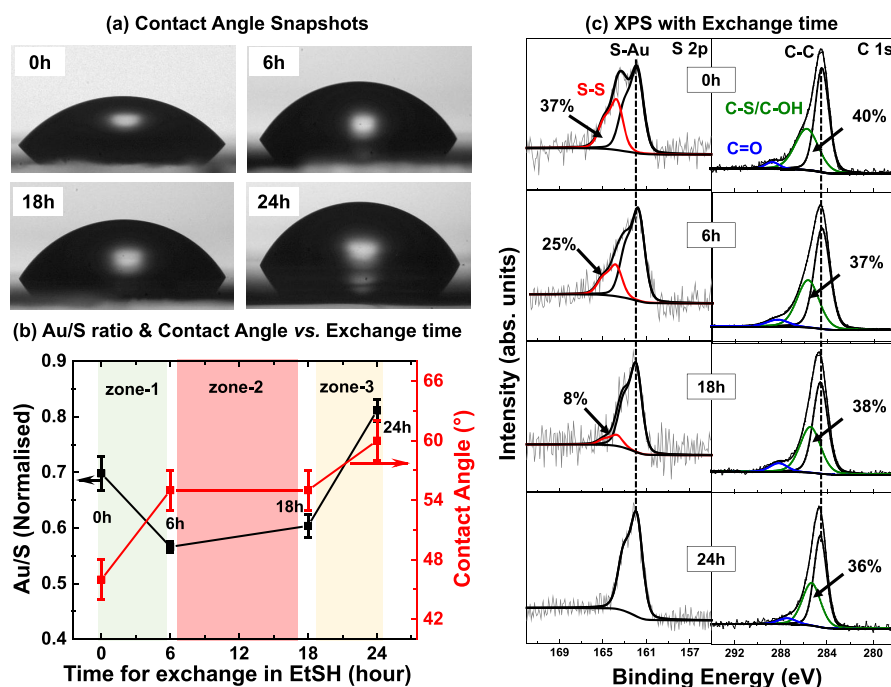


**Figure 3.** (a) Water contact angles on mixed monolayers of DTT grown from pure d-DTT SAM immersed in ethanolic solutions of EtSH for 0, 6, 18, and 24 h (exchange time). (b) Water contact angles (red) and Au/S ratios of integrated peak-areas normalized to SAMs of pure EtSH from XPS (black) versus exchange time for SAMs of DTT with EtSH. (c) XPS spectra of the substrates pictured in part a. The left column shows the S 2p core-level spectra, which comprise two doublets corresponding to Au—S bonds (black curve) and S—S bonds (red curve). The right column shows the C 1s core-level spectra comprising peaks corresponding to C—C bonds (black curve), C—S/C—OH bonds (green curve), and adventitious C=O species (blue curve).

of this peak to a specific chemical species enables quantitative measures of quality and deeper insight into the overall structure of a SAM and its interaction with the substrate upon which it self-assembles both pro- and retroactively.

For this study, we returned to dithiolreitol ((2S,3S)-1,4-bis(sulfanyl)butane-2,3-diol, DTT, see Figure 1) because it is well-established and readily forms stable, internal disulfide bonds. We grew SAMs of pure DTT and mixed monolayers of DTT and ethanethiol (EtSH)—which is effectively half of a DTT molecule—and varied the growth conditions while monitoring the S 2p core-level spectra. These data were further correlated to surface hydrophobicity and tunneling charge-transport through the thickness of the monolayers.

## RESULTS AND DISCUSSION

Owing to the formation of a stable six-membered ring, DTT readily forms internal disulfide bonds to form d-DTT, which can then be used to study Au—S interactions in the absence of free thiols. As depicted in Figure 1, d-DTT molecules can bind to the surface of Au in different configurations. Figure 1a,b depicts two possible binding modes in which the internal disulfide bond is preserved, and all Au—S interactions are, therefore, noncovalent. These are denoted as bidentate-physisorbed d-DTT, (bp)d-DTT (both sulfur atoms are interacting with Au), and monodentate-physisorbed d-DTT, (mp)d-DTT (only one sulfur atom is interacting with Au). In the third possible configuration, Figure 1c, both sulfur atoms are covalently bound to Au, which is denoted bidentate-chemisorbed DTT, (bc)-DTT. All of the SAMs of d-DTT on Au surfaces were prepared at room temperature from ethanolic solutions (0.1 mM) of d-DTT with varying immersion times, as explained below.

**XPS and Contact Angle Measurement.** To characterize the evolution of S/Au interactions, d-DTT SAMs were grown with different immersion times of 20, 120, and 720 min denoted as 20m, 120m, and 720m, respectively, as shown in Figure 2. The S 2p core-level spectra (shown in Figure 2c) comprise multiple doublets, confirming the presence of multiple oxidation states of S. The doublets peaked at 161.3, 162.0, and 163.6 eV correspond to S bound to Au hollow-sites (purple curve),<sup>43</sup> covalent Au—S bond (black curve),<sup>40,41,43</sup> and physisorbed disulfide (red curve),<sup>40,44,45</sup> respectively. The peak at 161.3 eV (purple curve) that is present in the spectra of 20m is absent in the 120m and 720m samples, which suggests that SAMs of d-DTT form by first filling Au hollow-sites to form a disordered monolayer.<sup>43</sup> However, rather than evolving into a single S—Au interaction with time, hollow-site bonding is replaced by a mix of Au—S and S—S species as indicated by the persistent presence of both red and black curves in 120m and 720m. Thus, at least two of the three species shown in Figure 1 persist at longer immersion times.

We ascribe the peak at 163.6 eV (red curve) exclusively to (bp)d-DTT using the following reasoning: Sulfur is more electronegative than hydrogen, meaning that the sulfur peak of a physisorbed organic thiol will appear at a lower binding energy than the corresponding disulfide, specifically in the range 163.0–164.0 eV,<sup>33,35,46,47</sup> thus, it cannot be physisorbed thiol. Moreover, d-DTT is a pure disulfide, meaning that the thiol protons would have to be provided by ethanol during the growth of the SAM. Formally, this is a redox reaction in which 2 equiv of H• are abstracted from ethanol to form the peroxide (CH<sub>3</sub>CH<sub>2</sub>O)<sub>2</sub> and DTT, which is unlikely. Finally, binding energies for physisorbed and free thiols have been reported at



163.2 eV.<sup>43,48</sup> The absence of any such peaks near or below the peak at 163.6 eV supports our hypothesis that the red curve corresponds to a single sulfur species, specifically (bp)d-DTT (Figure 1a).

Further evidence that (mp)d-DTT is not present in the SAMs can be found in the carbon spectra. The C 1s core-level region comprises multiple singlets: 284.5 eV (black curve),<sup>49</sup> 286.5 eV (green curve),<sup>50–52</sup> and 288.8 eV (blue curve),<sup>53–55</sup> corresponding to C—C bonds, C—S/C—OH bonds, and adventitious C=O species, respectively. Although the number and relative intensities of the peaks do not change significantly with immersion time, the green peak shifts to a lower binding energy by 0.5 eV between 20m and 720m, indicating an increase in electron density around the carbon atoms. This increase could be due to the formal reduction of sulfur (from S—S to Au<sup>δ+</sup>—S<sup>δ-</sup>), back-bonding in (bp)d-DTT (i.e., Au—S), hydrogen bonding between the OH groups as order within the SAM increases, or any combination thereof.

The density of organic thiols/disulfides in a SAM can be determined from the ratios of the integrated peak-areas of Au and S; the ratio of Au/S decreases as more thiol/disulfide adsorbs. Figure 2b compares this ratio for d-DTT (black squares), normalized to a SAM of EtSH grown for 720 min, showing that, indeed, the density of the SAM increases with immersion time commensurate with a decrease in water contact angle from the increasing density (and order) of the OH groups at the ambient interface. The water contact angle reaches a minimum of (40 ± 3)° for 720m, in agreement with the literature values.<sup>14</sup> Thus, although the water contact angle indicates a densely packed SAM of DTT, the persistence of the two doublets (black and red curves in Figure 2c) in the S 2p core-level region indicates that SAMs grown from d-DTT comprise a mixed phase of two distinct Au—S interactions.

For further insight into the nature of the two Au—S interactions, we prepared mixed monolayers of d-DTT and EtSH by exposing pure SAMs of DTT (120m) grown from d-DTT to 0.1 mM ethanolic solutions of EtSH for varying times. The data in Figure 3 are labeled with these exposure times (i.e., without varying the initial 120m used to form the starting pure SAM of DTT). The S 2p core-level region (which is identical to Figure 2b 120m) comprises two doublets at 161.8 eV<sup>40</sup> (black curve) and 163.6 eV (red curve) labeled as the Au—S and S—S bond. The relative amounts of S—S, calculated from the area under the red curve relative to the total S 2p core-level spectra, are (37 ± 2)%, (25 ± 3)%, (8 ± 2)%, and 0% for exchange times of 0, 6, 18, and 24 h, respectively. The overall trend shows a decrease in S—S with exchange time, eventually disappearing completely at 24 h. This trend indicates either that DTT is replaced completely by ethanethiol, or the S—S bond is reduced at the surface by exposure to ethanethiol, or a mixture of both. In any case, the commensurate reduction in the peak at 163.6 eV supports our hypothesis that this binding energy uniquely results from the presence of S—S bonds in the SAM.

The C 1s core-level spectra in Figure 3 comprise three different singlets corresponding (as in the pure SAMs of DTT in Figure 2) to C—C (black curve), C—S/C—OH (green curve), and adventitious C=O (blue curve). Interestingly, the peak of the green curve again shifts to lower binding energy by 0.5 eV between 0 and 6 h and then remains unchanged for rest of the samples. As with the pure SAMs, this shift reflects an increase in electron density on the carbon atoms and could be due to increasing hydrogen bonding at the ambient interface

and/or the formal reduction of sulfur. In addition, these SAMs are exposed to EtSH for increasing periods of time, which is reflected by the reduction in the relative amount of C—S/C—OH (in C 1s core-level spectra), sharply from 0 to 6 h, and then only slightly from 6 to 24 h. Thus, after pure SAMs of DTT are exposed to EtSH for 24 h, only one sulfur species (Au—S) is present in the XPS spectrum; however, the carbon spectra still show 36% of C—S/C—OH, indicating that DTT is still present.

Figure 3b shows the integrated peak-area ratios of Au/S (normalized to pure SAMs of EtSH) and water contact angles as a function of time exposed to EtSH. These data show that the exchange process can be divided into three different zones. In Zone-1 (0–6 h), the decreasing Au/S ratio and increasing contact angle suggest the replacement of weakly bound d-DTT by EtSH, decreasing the density of OH groups at the ambient interface. As described above, SAMs of DTT prepared by short immersion times (120m or 0 h sample) in solutions of d-DTT contain myriad defects and are disordered due to weakly bound d-DTT. Thus, after 6 h of exchange, EtSH fills the defects and displaces weakly bound d-DTT from the surface. In Zone-2 (6–8 h), the Au/S ratio increases slightly, while the water contact angle remains almost unchanged. This trend indicates that the amount of S (atoms) is nearly constant if not decreasing slightly, and the ratio of DTT:EtSH in the SAM remains constant. The XPS spectra (Figure 3c, red curve), however, indicate that the amount of S—S decreases by approximately 17% while the amount of C—S/C—OH remains constant. Together, these data suggest that over the 6–18 h time interval (Zone-2), the exchange process is dominated by the rearrangement of Au—S bonds on the surface. Over the same time interval, S—S bonds are cleaved at the surface, presumably reducing them to form covalent Au—S bonds. In Zone-3 (18–24 h), the Au/S increases sharply, and the water contact angle increases, indicating the desorption of DTT, presumably because it is displaced by EtSH. Over the same 18–24 h time interval, the S 2p core-level spectra show the complete loss of S—S, resulting in a single Au—S species in the mixed monolayer, but not complete replacement by EtSH, as substantial C—O/C—S peaks remain.

The O 1s spectrum (Figure S13a) confirms the presence of C—OH species at the ambient interface of all of the mixed SAMs, while there is no trace of C—OH in the spectra of SAMs of pure EtSH, which are shown in the bottom row of Figure S13b. The O 1s spectrum of mixed monolayers of DTT obtained after 6 h of exposure to EtSH is shifted to lower binding energies by 0.3 eV, consistent with the shift observed in the C 1s spectrum (Figure S12c). The variation of the O 1s (Figure S12a) spectral intensity with exchange time (0–24 h) further supports our assertions with respect to the relative amounts of C—S/C—OH species determined from the C 1s spectra (Figure S12c). Taken together, the data suggest that the disappearance of the peak at 163.6 eV occurs by different mechanisms. Exposure to EtSH results in the evolution of the peak at 162.0 eV in the S 2p core-level spectra; during these processes, the contact angle and Au:S ratio (Zone-3) clearly show the formal reduction of physisorbed S—S to chemisorbed Au—S, and we can unambiguously ascribe the peak at 163.6 eV in the core-level S 2p spectra to physisorbed S—S. The S 2p peaks of (mp)d-DTT and (bp)d-DTT are indistinguishable on the surface of Au only because of the resolution limit of XPS, but that does not preclude the assignment of the peak at 163.6 eV to S—S present on the surface of Au. Although we

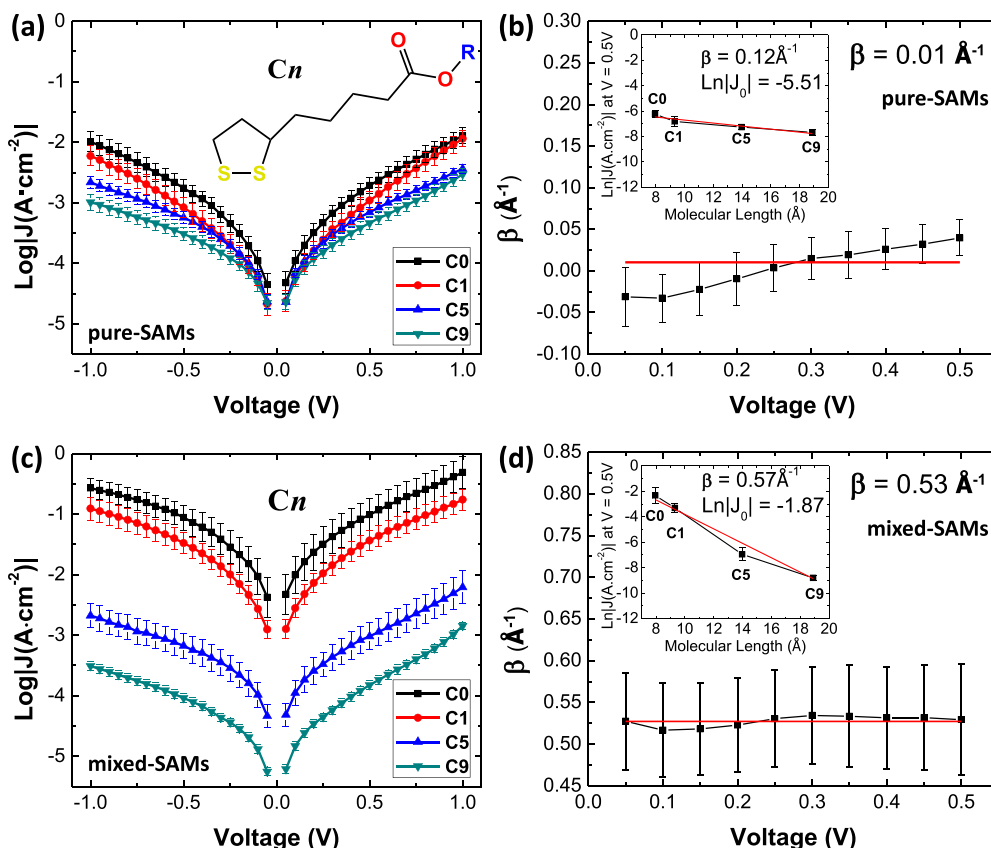


**Figure 4.** (a) Semilog plots of current density versus voltage ( $J$ - $V$ ) of SAMs of pure C0, C1, C5, and C9 molecules on Au<sup>TS</sup> measured with an EGaIn tip (the R groups and commensurate molecular lengths are defined in Table 1). (b) Values of  $\beta$  at different applied bias computed from the  $J$ - $V$  curves in panel a according to eq 1 showing no dependence on the length of the R group. (c) Semilog  $J$ - $V$  curves of the same series as panel a in mixed monolayers with octanethiol. (d) Value of  $\beta$  at different applied biases computed from the  $J$ - $V$  curves in panel c showing a clear dependence on the identity of the R group.

lack sufficient spectroscopic insight to prove the mechanism of disulfide–thiolate interconversion, Figure S11 presents a surface-analogue of disulfide metathesis in which EtSH converts S–S to Au–S, producing CH<sub>3</sub>CH<sub>2</sub>S<sub>2</sub> to balance the stoichiometry. Such metathesis is well-known in solution.<sup>56</sup>

**Tunneling Charge-transport Characterization.** The tunneling charge-transport properties of SAM simple organic thiols (e.g., aliphatic molecules) are sufficiently well-characterized that the injection current density  $J_0$ , tunneling decay coefficient  $\beta$  (from plots of  $\log J$  vs molecular length according to eq 1, where  $d$  is the width of the tunneling barrier), and conductance can be used to evaluate their properties.<sup>57</sup> For example, differences in the conductance of mono- and dithiol and disulfide moieties can be used to ascertain whether molecules are physisorbed or chemisorbed on Au.<sup>36</sup> We employed a similar strategy, using a series of esters derived from ( $\pm$ ) $\alpha$ -lipoic acid in which the thickness of the SAMs anchored identically to DTT can be varied. These compounds are labeled as C0 for the parent acid and C1, C5, and C9 for the methyl, pentyl, and nonyl esters, respectively, as shown in the inset of Figure 4a; e.g., R = CH<sub>3</sub> for C1. Table 1 summarizes the R groups and their theoretical length and the

**Table 1.** R Groups of the C<sub>n</sub> Series Shown in Figure 4a and Corresponding Molecular Lengths Calculated Using DFT and Measured in SAMs by XPS

abbreviation (C <sub>n</sub> )	R group	calculated molecular length (Å)	XPS pure SAM thickness (Å)
C0	H	7.91	7.0 ± 0.7
C1	CH <sub>3</sub>	9.25	8.0 ± 0.7
C5	C <sub>5</sub> H <sub>11</sub>	13.97	9.0 ± 0.8
C9	C <sub>9</sub> H <sub>19</sub>	18.90	16.0 ± 1.0

thicknesses of SAMs of their respective C<sub>n</sub> lipoic acid derivatives as determined by density functional theory (DFT) calculations and XPS.

$$J = J_0 e^{-\beta d} \quad (1)$$

Figure 4 summarizes the tunneling charge-transport properties of SAMs of the lipoic acid derivatives and the corresponding mixed monolayers with octanethiol on template-stripped Au (Au<sup>TS</sup>) substrates<sup>58</sup> using eutectic Ga–In (EGaIn) top-contacts.<sup>59</sup> In ordered, densely packed SAMs, the expectation is that the magnitude of  $J$  will vary

exponentially with molecular length according to the Simmons model (eq 1, eqs S2, S3, and S5)<sup>60</sup> for SAMs of *n*-alkanethiolates on Au  $\beta \approx 0.75 \text{ \AA}^{-1}$  and does not depend strongly on applied bias.<sup>61</sup> Although the lipoic acid series contains either a terminal carboxylic acid or internal ester, neither has a significant impact on  $\beta$ ;<sup>62,63</sup> however, Figure 4a,b shows almost no length-dependence, with  $\beta = 0.01 \text{ \AA}^{-1}$  and an approximately linear dependence on applied bias despite the very good agreement between the theoretical molecular length and experimental thicknesses of the SAMs (Table 1). The same data are shown in Figure 4c,d for mixed monolayers prepared by exposing pure SAMs of the lipoic acid derivatives (*C<sub>n</sub>*) to octanethiol. The mixed monolayers show a clear length-dependence and  $\beta = 0.53 \text{ \AA}^{-1}$ . Since the length of octanethiol is invariant, this value of  $\beta$  reflects the changing width of a tunneling barrier imposed by the R groups in the *C<sub>n</sub>* series. This is in agreement with the work by Yoon et al. showing the reduction of defect-induced conductance in mixed SAMs compared to pure SAMs.<sup>23</sup> In both the pure and mixed monolayers (Figure 4c,d), we observe rectification in *J*–*V* curves, most significantly for *C*9 SAMs, which indicates that this is a molecular property, consistent with observations by Whitesides et al.<sup>64,65</sup>

The S 2p core-level spectra (Figure 5) of SAMs of pure *C*1 exhibit two main doublets at 163.6 and 161.8 eV,

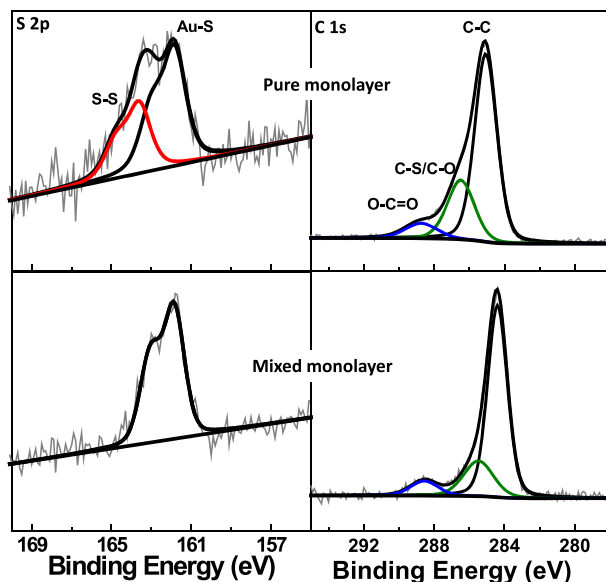


**Figure 5.** Representative XPS spectra of SAMs of pure *C*1 (top) and mixed monolayers of *C*1 and octanethiol (bottom). The left column shows the respective S 2p core-level spectra and fits revealing two doublets corresponding to Au–S (black) and S–S (red). The right column shows the respective C 1s core-level spectra and fits of the data revealing peaks ascribed to C–C (black), C–S/C–O (green), and O–C=O/C=O species (blue).

corresponding to S–S (40%) and Au–S (60%). In contrast, the mixed monolayers of *C*1 and octanethiol exhibit only one doublet at 161.8 eV, which is indicative of Au–S. The C 1s spectra are (qualitatively) unchanged in both mixed monolayers and pure SAMs. We chose octanethiol to form the mixed monolayers because it is slightly shorter than the molecular length of extended *C*0, which is a strategy that we have employed previously to ensure that the “background SAM” (octanethiol) does not directly contribute to the tunneling

barrier.<sup>40,66,67</sup> The recovery of the length-dependence of the tunneling currents is accompanied by the disappearance of the peak at 163.6 eV (labeled S–S in Figure 5). Jiang et al. demonstrated that even a relative intensity of 10% of a peak at 163.6 eV can alter the rectification ratio of tunneling junctions comprising ferrocene-terminated SAMs.<sup>68</sup> They ascribed the peak (correctly) to S–S and reasoned that the presence of disulfides in the SAM increases the leakage current, which reduces the rectification ratio. In our study, the relative intensity of the peak at 163.6 eV is 40% in pure SAMs of *C*1, which is significant enough to reduce  $\beta$  to near-zero. It also reduces the yield of working junctions to 30% (compared to 70% for the mixed monolayers), which implies a morphological effect as well, but our results support the hypothesis that the magnitude of a peak at 163.6 eV correlates to a contribution of nontunneling (leakage) current. However, eq 1 clearly shows that, whatever the morphological effects, they do not affect the thickness of the SAMs vis-à-vis the length of the R group. As we established above, exposure to octanethiol reduces S–S to Au–S; thus, we conclude that the peak at 163.6 eV is the result of physisorbed S–S, and that difference between that and chemisorbed Au–S is sufficient not just to affect  $\beta$  but also to mask the length-dependence entirely.

## CONCLUSIONS

The presence of a peak at  $(163.6 \pm 0.2) \text{ eV}$  in the S 2p<sub>3/2</sub> region of XPS spectra of SAMs grown from thiols is generally associated with SAMs of poor quality. Its presence is correlated to subtle changes in the physical properties of SAMs, including their behavior in tunneling junctions. However, it has not previously been assigned to a single, well-defined chemical species. We have shown, experimentally, that it results from the presence of physisorbed S–S species and that these species can be reduced to Au–S by exposure to an *n*-alkanethiol which, over the course of 24 h, eliminates S–S and reorganizes the SAM without replacing it. Our results also provide valuable insight into the role of disulfides in tunneling junctions comprising SAMs and reveal the surprising result that the chemical coupling of a SAM to the bottom electrode (and any associated conformational changes) can affect the length-dependence of tunneling currents to such an extent that the presence of disulfides can eliminate length-dependence entirely. While further study is needed to elucidate the exact nature of physisorbed S–S interactions, the assignment of the peaks at  $(163.6 \pm 0.2) \text{ eV}$  will aid these studies. The ubiquity of SAMs of thiols in science and engineering reflects their utility and versatility, and yet the nature of the chemical bonding between thiols and metal surfaces remains a source of controversy and a topic of research. The unambiguous elucidation of the chemical nature of the species that gives rise to the characteristic peak at  $(163.6 \pm 0.2) \text{ eV}$  enables further studies into the self-assembly process and the development of a more complete description of SAMs of thiols. The benefits of these insights are potentially as far-reaching as the impact of SAMs themselves.

## EXPERIMENTAL SECTION

**Patterned Gold Electrode (Au<sup>T5</sup>).** The 100 nm thick Au (99.99% pure, Schöne Edelmetaal B.V.) was thermally deposited (0.5–2 Å/s) onto a 3.5 in silicon wafer (purchased from ePAK). For template stripping, glass substrates were cleaned with soap (Multi Purpose Detergent, Teepol), acetone, and ethanol in an ultrasonic bath for 10 min. Once the substrates were dried with a N<sub>2</sub> gun, we



deposited a droplet of UV adhesive (Norland Optical Adhesive 61) on the glass substrate. Those were then placed on the metal surface, and the entire wafer was cured with UV light for 300 s (50% intensity, IntelliRay 600) to activate the adhesive.

**SAM Preparation and Treatments.** SAMs of DTT were prepared by immersing a freshly stripped Au<sup>TS</sup> substrate in a 1 mM solution of DTT in degassed, absolute ethanol (Macron Fine Chemicals) under Ar conditions, which was left for the specified incubation time in dark conditions. For *J*–*V* and XPS measurements, pure SAMs of the derivatives of (±) $\alpha$ -lipoic acid (C0–C9) were prepared from a 0.1 mM ethanolic solution of the respective molecules for 12 h. Mixed SAMs were prepared in two steps, where first, Au<sup>TS</sup> substrates were immersed in a 0.1 mM ethanolic solution for 120 min of the respective molecules, and then, second, these pure SAMs were immersed in 1 mM ethanolic solution of octanethiol for 24 h at room temperature. All these samples were then washed three times in 3 mL of ethanol and blown dry with Ar gas.

**EGaIn/SAM/Au<sup>TS</sup> Measurements.** The *J*–*V* traces were collected using a setup (described elsewhere<sup>69</sup>) placed inside a flowbox (N<sub>2</sub> atm of <5% relative humidity and O<sub>2</sub> 1–3%) using LabView (National Instruments) with 5 sweeping cycles between +1 V and –1 V using a subfemtoamperometer (6430 SourceMeter, Keithley) and were analyzed using the GaussFit package.

**XPS Analysis.** XPS was performed using a Surface Science SSX-100 ESCA instrument, using monochromatic Al K $\alpha$  as the X-ray source ( $h\nu = 1486.6$  eV). The pressure inside the measurement chamber was maintained below 10<sup>–9</sup> mbar. The electron takeoff angle with respect to the surface normal was 37°. The diameter of the analyzed area was 1000  $\mu$ m; the energy resolution was set to 1.1 eV to minimize data acquisition times. XPS spectra were analyzed with the fitting program Winspec (from LISE laboratory of the Facultés Universitaires Notre-Dame de la Paix, Namur, Belgium).

**Computational Methodologies.** To calculate the molecular lengths, geometry optimizations were performed using the Orca 4.0.1 software package.<sup>70,71</sup> We used the B3LYP functional in combination with the default def2-SVP basis sets, and the lengths of the optimized geometry of the C $n$  molecules were measured using the distance between the terminal C/O atom of the alkyl chain and the sulfur atom next to the carbon atom to which the alkyl tail is attached.

## ■ ASSOCIATED CONTENT

### Supporting Information

The Supporting Information is available free of charge at <https://pubs.acs.org/doi/10.1021/jacs.0c06508>.

Synthetic detail and full characterization data for all new compounds, description of measurement techniques, and additional spectroscopic data on monolayers (PDF)

## ■ AUTHOR INFORMATION

### Corresponding Authors

**Petra Rudolf** – Zernike Institute for Advanced Materials, 9747 AG Groningen, The Netherlands; [orcid.org/0000-0002-4418-1769](https://orcid.org/0000-0002-4418-1769); Email: [p.rudolf@rug.nl](mailto:p.rudolf@rug.nl)

**Ryan C. Chiechi** – Stratingh Institute for Chemistry, University of Groningen, 9747 AG Groningen, The Netherlands; Zernike Institute for Advanced Materials, 9747 AG Groningen, The Netherlands; [orcid.org/0000-0002-0895-2095](https://orcid.org/0000-0002-0895-2095); Email: [r.c.chiechi@rug.nl](mailto:r.c.chiechi@rug.nl)

### Authors

**Sumit Kumar** – Stratingh Institute for Chemistry, University of Groningen, 9747 AG Groningen, The Netherlands; Zernike Institute for Advanced Materials, 9747 AG Groningen, The Netherlands

**Saurabh Soni** – Stratingh Institute for Chemistry, University of Groningen, 9747 AG Groningen, The Netherlands; Zernike

Institute for Advanced Materials, 9747 AG Groningen, The Netherlands; [orcid.org/0000-0002-8159-9128](https://orcid.org/0000-0002-8159-9128)

**Wojciech Danowski** – Stratingh Institute for Chemistry, University of Groningen, 9747 AG Groningen, The Netherlands; Zernike Institute for Advanced Materials, 9747 AG Groningen, The Netherlands; [orcid.org/0000-0002-8588-8912](https://orcid.org/0000-0002-8588-8912)

**Carlijn L. F. van Beek** – Stratingh Institute for Chemistry, University of Groningen, 9747 AG Groningen, The Netherlands; Zernike Institute for Advanced Materials, 9747 AG Groningen, The Netherlands

**Ben L. Feringa** – Stratingh Institute for Chemistry, University of Groningen, 9747 AG Groningen, The Netherlands; Zernike Institute for Advanced Materials, 9747 AG Groningen, The Netherlands; [orcid.org/0000-0003-0588-8435](https://orcid.org/0000-0003-0588-8435)

Complete contact information is available at: <https://pubs.acs.org/doi/10.1021/jacs.0c06508>

## Notes

The authors declare no competing financial interest.

## ■ ACKNOWLEDGMENTS

R.C.C. and S.K. acknowledge the European Research Council for the ERC Starting Grant 335473 (MOLECSYNCON). S.S. acknowledges the Zernike Institute for Advanced Materials. We thank the Center for Information Technology of the University of Groningen for their support and for providing access to the Peregrine high-performance computing cluster.

## ■ REFERENCES

- (1) Häkkinen, H. The gold–sulfur interface at the nanoscale. *Nat. Chem.* **2012**, *4*, 443–455.
- (2) Love, J. C.; Estroff, L. A.; Kriebel, J. K.; Nuzzo, R. G.; Whitesides, G. M. Self-Assembled Monolayers of Thiolates on Metals as a Form of Nanotechnology. *Chem. Rev.* **2005**, *105*, 1103–1170.
- (3) Boisselier, E.; Astruc, D. Gold Nanoparticles in Nanomedicine: Preparations, Imaging, Diagnostics, Therapies and Toxicity. *Chem. Soc. Rev.* **2009**, *38*, 1759–1782.
- (4) Kumar, A.; Biebuyck, H. A.; Whitesides, G. M. Patterning Self-Assembled Monolayers: Applications in Materials Science. *Langmuir* **1994**, *10*, 1498–1511.
- (5) Liao, W.-S.; Cheunkar, S.; Cao, H. H.; Bednar, H. R.; Weiss, P. S.; Andrews, A. M. Subtractive Patterning via Chemical Lift-Off Lithography. *Science* **2012**, *337*, 1517–1521.
- (6) Motesharei, K.; Myles, D. C. Molecular Recognition on Functionalized Self-Assembled Monolayers of Alkanethiols on Gold. *J. Am. Chem. Soc.* **1998**, *120*, 7328–7336.
- (7) Schliwa, M.; Woehlke, G. Molecular Motors. *Nature* **2003**, *422*, 759–765.
- (8) Yao, H.; Miki, K.; Nishida, N.; Sasaki, A.; Kimura, K. Large Optical Activity of Gold Nanocluster Enantiomers Induced by a Pair of Optically Active Penicillamines. *J. Am. Chem. Soc.* **2005**, *127*, 15536–15543.
- (9) Gautier, C.; Bürgi, T. Chiral N-Isobutyryl-Cysteine Protected Gold Nanoparticles: Preparation, Size Selection, and Optical Activity in the UV-vis and Infrared. *J. Am. Chem. Soc.* **2006**, *128* (34), 11079–11087.
- (10) Yeung, S. Y.; Ederth, T.; Pan, G.; Cicenaitė, J.; Cárdenas, M.; Arnebrant, T.; Sellergren, B. Reversible Self-Assembled Monolayers (rSAMs) as Robust and Fluidic Lipid Bilayer Mimics. *Langmuir* **2018**, *34*, 4107–4115.
- (11) Sethuraman, A.; Han, M.; Kane, R. S.; Belfort, G. Effect of Surface Wettability on the Adhesion of Proteins. *Langmuir* **2004**, *20*, 7779–7788.



- (12) Samuel, B.; Zhao, H.; Law, K.-Y. Study of Wetting and Adhesion Interactions Between Water and Various Polymer and Superhydrophobic Surfaces. *J. Phys. Chem. C* **2011**, *115*, 14852–14861.
- (13) Ramachandran, S.; Tsai, B.-L.; Blanco, M.; Chen, H.; Tang, Y.; Goddard, W. A. Self-Assembled Monolayer Mechanism for Corrosion Inhibition of Iron by Imidazolines. *Langmuir* **1996**, *12*, 6419–6428.
- (14) Nuzzo, R. G.; Allara, D. L. Adsorption of Bifunctional Organic Disulfides on Gold Surfaces. *J. Am. Chem. Soc.* **1983**, *105*, 4481–4483.
- (15) Nuzzo, R. G.; Zegarski, B. R.; Dubois, L. H. Fundamental Studies of the Chemisorption of Organosulfur Compounds on Gold(111). Implications for Molecular Self-Assembly on Gold Surfaces. *J. Am. Chem. Soc.* **1987**, *109*, 733–740.
- (16) Bain, C. D.; Evall, J.; Whitesides, G. M. Formation of Monolayers by the Coadsorption of Thiols on Gold: Variation in the Head Group, Tail Group, and Solvent. *J. Am. Chem. Soc.* **1989**, *111*, 7155–7164.
- (17) Bain, C. D.; Biebuyck, H. A.; Whitesides, G. M. Comparison of Self-Assembled Monolayers on Gold: Coadsorption of Thiols and Disulfides. *Langmuir* **1989**, *5*, 723–727.
- (18) Ulman, A. *Self-Assembled Monolayers of Thiols; Thin Films*; Academic Press, 1998; Vol. 24.
- (19) Xue, Y.; Li, X.; Li, H.; Zhang, W. Quantifying thiol–gold interactions towards the efficient strength control. *Nat. Commun.* **2014**, *5*, 1–9.
- (20) Kong, G. D.; Byeon, S. E.; Park, S.; Song, H.; Kim, S.-Y.; Yoon, H. J. Mixed Molecular Electronics: Tunneling Behaviors and Applications of Mixed Self-Assembled Monolayers. *Advanced Electronic Materials* **2020**, *6*, 1901157.
- (21) Jin, J.; Kong, G. D.; Yoon, H. J. Deconvolution of Tunneling Current in Large-Area Junctions Formed with Mixed Self-Assembled Monolayers. *J. Phys. Chem. Lett.* **2018**, *9*, 4578–4583.
- (22) Kong, G. D.; Kim, M.; Cho, S. J.; Yoon, H. J. Gradients of Rectification: Tuning Molecular Electronic Devices by the Controlled Use of Different-Sized Diluents in Heterogeneous Self-Assembled Monolayers. *Angew. Chem., Int. Ed.* **2016**, *55*, 10307–10311.
- (23) Kong, G. D.; Jin, J.; Thuo, M.; Song, H.; Joung, J. F.; Park, S.; Yoon, H. J. Elucidating the Role of Molecule–Electrode Interfacial Defects in Charge Tunneling Characteristics of Large-Area Junctions. *J. Am. Chem. Soc.* **2018**, *140*, 12303–12307.
- (24) Ben Amara, F.; Dionne, E. R.; Kassir, S.; Pellerin, C.; Badia, A. Molecular Origin of the Odd–Even Effect of Macroscopic Properties of n-Alkanethiolate Self-Assembled Monolayers: Bulk or Interface? *J. Am. Chem. Soc.* **2020**, *142*, 13051–13061.
- (25) Chen, J.; Giroux, T. J.; Nguyen, Y.; Kadoma, A. A.; Chang, B. S.; VanVeller, B.; Thuo, M. M. Understanding interface (odd–even) effects in charge tunneling using a polished EGaIn electrode. *Phys. Chem. Chem. Phys.* **2018**, *20*, 4864–4878.
- (26) Chen, J.; Chang, B.; Oyola-Reynoso, S.; Wang, Z.; Thuo, M. Quantifying Gauche Defects and Phase Evolution in Self-Assembled Monolayers through Sessile Drops. *ACS Omega* **2017**, *2*, 2072–2084.
- (27) Rooth, M.; Shaw, A. M. pH-Controlled Formation Kinetics of Self-Assembled Layers of Thiocetic Acid on Gold Nanoparticles. *J. Phys. Chem. C* **2007**, *111*, 15363–15369.
- (28) Han, S.; Park, H.; Han, J. W.; Yoshizawa, K.; Hayashi, T.; Hara, M.; Noh, J. Solvent Effect on the Formation of Octaneselenocyanate Self-Assembled Monolayers on Au(111). *J. Nanosci. Nanotechnol.* **2019**, *19*, 4795–4798.
- (29) Ivashenko, O.; van Herpt, J.; Feringa, B.; Browne, W.; Rudolf, P. Rapid Reduction of Self-Assembled Monolayers of a Disulfide Terminated Para-Nitrophenyl Alkyl Ester on Roughened Au Surfaces During XPS Measurements. *Chem. Phys. Lett.* **2013**, *559*, 76–81.
- (30) Kong, G. D.; Yoon, H. J. Influence of Air-Oxidation on Rectification in Thiol-Based Molecular Monolayers. *J. Electrochem. Soc.* **2016**, *163*, G115–G121.
- (31) Lee, L. Y. S.; Lennox, R. B. Electrochemical Desorption of N-Alkylthiol SAMs on Polycrystalline Gold: Studies Using a Ferrocenylalkylthiol Probe. *Langmuir* **2007**, *23*, 292–296.
- (32) Neuman, K. C.; Nagy, A. Single-Molecule Force Spectroscopy: Optical Tweezers, Magnetic Tweezers and Atomic Force Microscopy. *Nat. Methods* **2008**, *5*, 491–505.
- (33) Martínez, L.; Carrascosa, L. G.; Huttel, Y.; Lechuga, L. M.; Román, E. Influence of the Linker Type on the Au–S Binding Properties of Thiol and Disulfide-Modified DNA Self-Assembly on Polycrystalline Gold. *Phys. Chem. Chem. Phys.* **2010**, *12*, 3301–3308.
- (34) Souto, M.; Yuan, L.; Morales, D. C.; Jiang, L.; Ratera, I.; Nijhuis, C. A.; Veciana, J. Tuning the Rectification Ratio by Changing the Electronic Nature (Open-Shell and Closed-Shell) in Donor–Acceptor Self-Assembled Monolayers. *J. Am. Chem. Soc.* **2017**, *139*, 4262–4265.
- (35) Vericat, C.; Vela, M. E.; Benitez, G.; Carro, P.; Salvarezza, R. C. Self-Assembled Monolayers of Thiols and Dithiols on Gold: New Challenges for a Well-Known System. *Chem. Soc. Rev.* **2010**, *39*, 1805–1834.
- (36) Inkpen, M. S.; Liu, Z.-F.; Li, H.; Campos, L. M.; Neaton, J. B.; Venkataraman, L. Non-Chemisorbed Gold-Sulfur Binding Prevails in Self-Assembled Monolayers. *Nat. Chem.* **2019**, *11*, 351–358.
- (37) Zotti, L. A.; Kirchner, T.; Cuevas, J.-C.; Pauly, F.; Huhn, T.; Scheer, E.; Erbe, A. Revealing the Role of Anchoring Groups in the Electrical Conduction Through Single-Molecule Junctions. *Small* **2010**, *6*, 1529–1535.
- (38) Zharnikov, M.; Grunze, M. Spectroscopic Characterization of Thiol-Derived Self-Assembling Monolayers. *J. Phys.: Condens. Matter* **2001**, *13*, 11333–11365.
- (39) Rodriguez-Douton, M. J.; Mannini, M.; Armelao, L.; Barra, A.-L.; Tancini, E.; Sessoli, R.; Cornia, A. One-Step Covalent Grafting of Fe<sub>4</sub> Single-Molecule Magnet Monolayers on Gold. *Chem. Commun.* **2011**, *47*, 1467–1469.
- (40) Kumar, S.; van Herpt, J. T.; Gengler, R. Y. N.; Feringa, B. L.; Rudolf, P.; Chiechi, R. C. Mixed Monolayers of Spiropyran Maximize Tunneling Conductance Switching by Photoisomerization at the Molecule–Electrode Interface in EGaIn Junctions. *J. Am. Chem. Soc.* **2016**, *138*, 12519–12526.
- (41) Ivashenko, O.; van Herpt, J. T.; Feringa, B. L.; Rudolf, P.; Browne, W. R. UV/Vis and NIR Light-Responsive Spiropyran Self-Assembled Monolayers. *Langmuir* **2013**, *29*, 4290–4297.
- (42) Hamoudi, H.; Esaulov, V. A. Selfassembly of  $\alpha,\omega$ -Dithiols on Surfaces and Metal Dithiol Heterostructures. *Ann. Phys.* **2016**, *528*, 242–263.
- (43) Ishida, T.; Hara, M.; Kojima, I.; Tsuneda, S.; Nishida, N.; Sasabe, H.; Knoll, W. High Resolution X-Ray Photoelectron Spectroscopy Measurements of Octadecanethiol Self-Assembled Monolayers on Au(111). *Langmuir* **1998**, *14*, 2092–2096.
- (44) Cortés, E.; Rubert, A. A.; Benitez, G.; Carro, P.; Vela, M. E.; Salvarezza, R. C. Enhanced Stability of Thiolate Self-Assembled Monolayers (SAMs) on Nanostructured Gold Substrates. *Langmuir* **2009**, *25*, 5661–5666.
- (45) Watcharinyanon, S.; Nilsson, D.; Moons, E.; Shaporenko, A.; Zharnikov, M.; Albinsson, B.; Mårtensson, J.; Johansson, L. S. O. A Spectroscopic Study of Self-Assembled Monolayer of Porphyrin-Functionalized Oligo(phenyleneethynylene)s on Gold: The Influence of the Anchor Moiety. *Phys. Chem. Chem. Phys.* **2008**, *10*, 5264–5275.
- (46) Grumelli, D.; Cristina, L. J.; Maza, F. L.; Carro, P.; Ferrón, J.; Kern, K.; Salvarezza, R. C. Thiol Adsorption on the Au(100)-Hex and Au(100)-(1 × 1) Surfaces. *J. Phys. Chem. C* **2015**, *119*, 14248–14254.
- (47) Park, J.-W.; Shumaker-Parry, J. S. Strong Resistance of Citrate Anions on Metal Nanoparticles to Desorption Under Thiol Functionalization. *ACS Nano* **2015**, *9*, 1665–1682.
- (48) Cristina, L. J.; Ruano, G.; Salvarezza, R.; Ferrón, J. Thermal Stability of Self-Assembled Monolayers of N-Hexanethiol on Au(111)-(1 × 1) and Au(001)-(1 × 1). *J. Phys. Chem. C* **2017**, *121*, 27894–27904.
- (49) Rani, J. R.; Lim, J.; Oh, J.; Kim, D.; Lee, D.; Kim, J.-W.; Shin, H. S.; Kim, J. H.; Jun, S. C. Substrate and Buffer Layer Effect on the Structural and Optical Properties of Graphene Oxide Thin Films. *RSC Adv.* **2013**, *3*, 5926–5936.

- (50) Ivashenko, O.; Logtenberg, H.; Areephong, J.; Coleman, A. C.; Wesenhagen, P. V.; Geertsema, E. M.; Heureux, N.; Feringa, B. L.; Rudolf, P.; Browne, W. R. Remarkable Stability of High Energy Conformers in Self-Assembled Monolayers of a Bistable Electro- And Photoswitchable Overcrowded Alkene. *J. Phys. Chem. C* **2011**, *115*, 22965–22975.
- (51) Wang, Z.; Dong, Y.; Li, H.; Zhao, Z.; Bin Wu, H.; Hao, C.; Liu, S.; Qiu, J.; Lou, X. W. (Enhancing Lithium-Sulphur Battery Performance by Strongly Binding the Discharge Products on Amino-Functionalized Reduced Graphene Oxide. *Nat. Commun.* **2014**, *5*, 5002.
- (52) Wang, H.; Zhou, H.; Gestos, A.; Fang, J.; Niu, H.; Ding, J.; Lin, T. Robust, Electro-Conductive, Self-Healing Superamphiphobic Fabric Prepared by One-Step Vapour-Phase Polymerisation of Poly(3,4-Ethylenedioxythiophene) in the Presence of Fluorinated Decyl Polyhedral Oligomeric Silsesquioxane and Fluorinated Alkyl Silane. *Soft Matter* **2013**, *9*, 277–282.
- (53) Bazylewski, P.; Boukhalov, D. W.; Kukhareno, A. I.; Kurmaev, E. Z.; Hunt, A.; Moewes, A.; Lee, Y. H.; Cholakh, S. O.; Chang, G. S. The Characterization of Co-Nanoparticles Supported on Graphene. *RSC Adv.* **2015**, *5*, 75600–75606.
- (54) Tao, C.-a.; Wang, J.; Qin, S.; Lv, Y.; Long, Y.; Zhu, H.; Jiang, Z. Fabrication of pH-sensitive Graphene Oxide–Drug Supramolecular Hydrogels as Controlled Release Systems. *J. Mater. Chem.* **2012**, *22*, 24856–24861.
- (55) Haubner, K.; Murawski, J.; Olk, P.; Eng, L. M.; Ziegler, C.; Adolph, B.; Jaehne, E. The Route to Functional Graphene Oxide. *ChemPhysChem* **2010**, *11*, 2131–2139.
- (56) Lees, W. J.; Whitesides, G. M. Equilibrium constants for thiol-disulfide interchange reactions: a coherent, corrected set. *J. Org. Chem.* **1993**, *58*, 642–647.
- (57) Vilan, A.; Aswal, D.; Cahen, D. Large-Area, Ensemble Molecular Electronics: Motivation and Challenges. *Chem. Rev.* **2017**, *117*, 4248–4286.
- (58) Weiss, E. A.; Kaufman, G. K.; Kriebel, J. K.; Li, Z.; Schalek, R.; Whitesides, G. M. Si/SiO<sub>2</sub>-Templated Formation of Ultraflat Metal Surfaces on Glass, Polymer, and Solder Supports: Their Use as Substrates for Self-Assembled Monolayers. *Langmuir* **2007**, *23*, 9686–9694.
- (59) Chiechi, R. C.; Weiss, E. A.; Dickey, M. D.; Whitesides, G. M. Eutectic Gallium-Indium (EGaIn): A Moldable Liquid Metal for Electrical Characterization of Self-Assembled Monolayers. *Angew. Chem., Int. Ed.* **2008**, *47*, 142–144.
- (60) Wang, W.; Lee, T.; Reed, M. A. Mechanism of Electron Conduction in Self-Assembled Alkanethiol Monolayer Devices. *Phys. Rev. B: Condens. Matter Mater. Phys.* **2003**, *68*, 035416.
- (61) Simeone, F. C.; Yoon, H. J.; Thuo, M. M.; Barber, J. R.; Smith, B.; Whitesides, G. M. Defining the Value of Injection Current and Effective Electrical Contact Area for EGaIn-Based Molecular Tunneling Junctions. *J. Am. Chem. Soc.* **2013**, *135*, 18131–18144.
- (62) Thuo, M. M.; Reus, W. F.; Simeone, F. C.; Kim, C.; Schulz, M. D.; Yoon, H. J.; Whitesides, G. M. Replacing -CH<sub>2</sub>CH<sub>2</sub>- With -CONH- Does Not Significantly Change Rates of Charge Transport Through AgTS-SAM//Ga<sub>2</sub>O<sub>3</sub>/EGaIn Junctions. *J. Am. Chem. Soc.* **2012**, *134*, 10876–10884.
- (63) Ai, Y.; Kovalchuk, A.; Qiu, X.; Zhang, Y.; Kumar, S.; Wang, X.; Kühnel, M.; Nørgaard, K.; Chiechi, R. C. In-Place Modulation of Rectification in Tunneling Junctions Comprising Self-Assembled Monolayers. *Nano Lett.* **2018**, *18*, 7552–7559.
- (64) Yoon, H. J.; Shapiro, N. D.; Park, K. M.; Thuo, M. M.; Soh, S.; Whitesides, G. M. The Rate of Charge Tunneling through Self-Assembled Monolayers Is Insensitive to Many Functional Group Substitutions. *Angew. Chem., Int. Ed.* **2012**, *51*, 4658–4661.
- (65) Baghbanzadeh, M.; Belding, L.; Yuan, L.; Park, J.; Al-Sayah, M. H.; Bowers, C. M.; Whitesides, G. M. Dipole-Induced Rectification Across AgTS/SAM//Ga<sub>2</sub>O<sub>3</sub>/EGaIn Junctions. *J. Am. Chem. Soc.* **2019**, *141*, 8969–8980.
- (66) Kumar, S.; Merelli, M.; Danowski, W.; Rudolf, P.; Feringa, B. L.; Chiechi, R. C. Chemical Locking in Molecular Tunneling Junctions Enables Nonvolatile Memory With Large On–Off Ratios. *Adv. Mater.* **2019**, *31*, 1807831.
- (67) Qiu, L.; Zhang, Y.; Krijger, T. L.; Qiu, X.; Hof, P. v.; Hummelen, J. C.; Chiechi, R. C. Rectification of current responds to incorporation of fullerenes into mixed-monolayers of alkanethiolates in tunneling junctions. *Chem. Sci.* **2017**, *8*, 2365–2372.
- (68) Jiang, L.; Yuan, L.; Cao, L.; Nijhuis, C. A. Controlling Leakage Currents: The Role of the Binding Group and Purity of the Precursors for Self-Assembled Monolayers in the Performance of Molecular Diodes. *J. Am. Chem. Soc.* **2014**, *136*, 1982–1991.
- (69) Fracasso, D.; Valkenier, H.; Hummelen, J. C.; Solomon, G. C.; Chiechi, R. C. Evidence for Quantum Interference in SAMs of Arylethynylene Thiolates in Tunneling Junctions With Eutectic Ga–In (EGaIn) Top-Contacts. *J. Am. Chem. Soc.* **2011**, *133*, 9556–9563.
- (70) Neese, F. The ORCA Program System. *Wiley Interdiscip. Rev.: Comput. Mol. Sci.* **2012**, *2*, 73–78.
- (71) Neese, F. Software update: the ORCA program system, version 4.0. *Wiley Interdiscip. Rev.: Comput. Mol. Sci.* **2018**, *8*, e1327.